Magnetic torque and heat capacity measurements on TPP[Fe(Pc)(CN)$_2$]$_2$

Hiroyuki Tajima, Gosuke Yoshida, and Masaki Matsuda
Institute for Solid State Physics, The University of Tokyo, Kashiwa, Chiba 277-8581, Japan

Kazumi Nara, Koji Kajita, and Yutaka Nishio
Department of Physics, Toho University, Funabashi, Chiba 274-8510, Japan

Noriaki Hanasaki
Department of Physics, Faculty of Science, Okayama University, Okayama 700-8530, Japan

Toshio Naito and Tamotsu Inabe
Division of Chemistry, Graduate School of Science, Hokkaido University, Kita-ku, Sapporo 060-0810, Japan
(Received 15 March 2008; published 26 August 2008)

Magnetic torque and heat capacity measurements on TPP[Fe(Pc)(CN)$_2$]$_2$ are reported. The torque curves for the magnetic field rotated within the *ab* plane have a fourfold symmetry, exhibiting inversions around 13 and 27 K. The heat capacity exhibits a broad peak around $T=16.5$ K. By applying the magnetic field along the *c* axis, the maximum value of the heat capacity is enhanced below 20 K. These results, as well as the magnetic susceptibility, were analyzed by employing a numerical calculation based on the anisotropic Heisenberg model in one dimension. The analyses revealed that: (i) the peak in the magnetic-susceptibility data around 25 K is due to an antiferromagnetic short-range order (SRO) formation associated with *d* electrons, and (ii) π electrons fall into an antiferromagnetic state below 13 K. The spin-flop field of π electrons is approximately 80 kOe at 9 K.

DOI: 10.1103/PhysRevB.78.064424 PACS number(s): 75.50.Xx, 75.30.Gw, 75.47.De

I. INTRODUCTION

The title compound TPP[Fe(Pc)(CN)$_2$]$_2$ is a one-dimensional molecular conductor that exhibits giant negative magnetoresistance (GNMR) [$R(H)/R(0)<0.01$ at $T=20$ K and $H=350$ kOe].[1,2] Here, Pc and TPP denote phthalocyanine and tetraphenylphosphonium, respectively. This GNMR is an interesting phenomenon both experimentally and theoretically,[3] since it is not caused by a sharp transition such as the field-induced metal-insulator transition observed in the manganese oxides[4] and λ-(BETS)$_2$FeCl$_4$.[5] It is highly anisotropic for the magnetic-field direction, reflecting the molecular orientation of [Fe(Pc)(CN)$_2$]. Similar GNMR phenomena are observed in other salts of [Fe(Pc)(CN)$_2$].[6]

Figure 1 shows the molecular structure of [Fe(Pc)(CN)$_2$]. The Pc ring (see the figure) provides the π electrons that form a conduction band in the solid state. The Fe(III) at the center of the ring is in the low-spin state with $S=1/2$. Because of the fourfold symmetry of [Fe(Pc)(CN)$_2$], the orbital magnetic moment of Fe(III) is not completely quenched. Consequently, Fe(III) behaves as a local magnetic moment with highly anisotropic *g* factors. ($g_{xx}=0.52$, $g_{yy}=1.11$, and $g_{zz}=3.62$ in the case of PNP[Fe(Pc)(CN)$_2$].[7]) There are strong interaction between the π electrons in the Pc ring and the *d* electrons of Fe(III). This intramolecular *d*-π interaction is the origin of the GNMR phenomena in molecular conductors of [Fe(Pc)(CN)$_2$]. In fact, the anisotropy of the GNMR for the magnetic-field orientation is qualitatively explained by taking account of the large *g*-factor anisotropy of Fe(III).[6]

In order to study this GNMR phenomenon in detail, the magnetic states of both the *d*- and the π-electron systems in [Fe(Pc)(CN)$_2$] salts should be clarified on the basis of microscopic pictures. However, attempts to do so have not yet succeeded.

Figure 2 shows the temperature dependence of the magnetic susceptibility for TPP[Fe(Pc)(CN)$_2$]$_2$, reported elsewhere.[1,8] The susceptibility is highly anisotropic for the field direction. Since the *z* axis (∥CN axis: the direction of the largest *g* factor) is almost perpendicular to the crystallographic *c* axis, the magnetic susceptibility for $B\perp c$ is much larger than that for $B\parallel c$. The $B\perp c$ susceptibility exhibits a peak around 25 K, gradually decreases down to 13 K, and then abruptly increases. The peak around 25 K is missing in the $B\parallel c$ susceptibility. Below 6 K, spontaneous magnetization was observed for a sample cooled down in a magnetic field. (See the inset.) A similar peak around 25 K as well as spontaneous magnetization was also observed in the magnetic-susceptibility data of the powder samples of PXX[Fe(Pc)(CN)$_2$] (Ref. 9) and PTMA$_x$[Fe(Pc)(CN)$_2$]$_y$(CH$_3$CN).[10]

In this paper, we report experimental studies on magnetic torque and heat capacity for TPP[Fe(Pc)(CN)$_2$]$_2$. We present

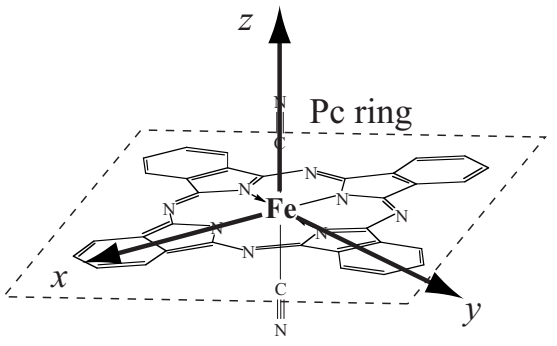

FIG. 1. Molecular structure of [Fe(Pc)(CN)$_2$] and the definition of *xyz* principal axes in the *g* tensor of Fe(III) in [Fe(Pc)(CN)$_2$].

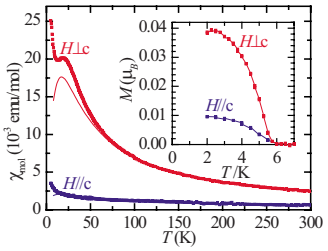

FIG. 2. (Color online) Temperature dependence of the magnetic susceptibility of TPP[Fe(Pc)(CN)$_2$]$_2$. The inset shows the spontaneous magnetization measured at the zero field for the sample cooled in the field of 55 kOe. The solid lines show the calculations of magnetic susceptibility based on the anisotropic Heisenberg model [Eq. (1)]. See the details in Sec. IV.

a comprehensive analysis of magnetic susceptibility, heat capacity, and magnetic torque for this compound based on the anisotropic Heisenberg model in one dimension. We demonstrate that this model well explains the magnetic properties above 13 K including the maximum of the susceptibility around 25 K.

II. EXPERIMENT

Magnetic torque was measured using commercially available cantilevers (NPX1CTP003 and NPX1CTP004, Seiko Instruments). We developed the experimental technique originally reported by Ohmichi and Osada.[11] The details of our technique will be published elsewhere. The magnetic field was rotated within the *ab* plane. Figure 3 illustrates the crystal structure of the title compound ($P4_2/n$: $a=b=21.772$ Å and $c=7.448$ Å) and the angle θ which defines the field direction.[12] Note that the starting point of θ is parallel to the projection of the CN bond on the *ab* plane, as indicated by the broken line. The tilt of the projection from the *a* axis is approximately 59.5°. The positive or negative

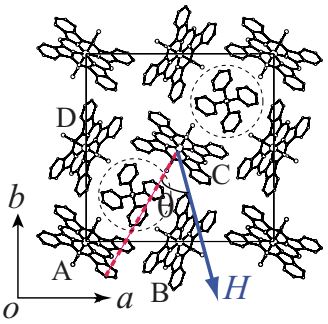

FIG. 3. (Color online) The crystal structure of TPP[Fe(Pc)(CN)$_2$]$_2$ within the *ab* plane and the definition of the angle θ in the magnetic torque measurements. The molecules encircled by dotted lines are TPP cations [$P(C_6H_5)_4^+$ =tetraphenylphosphonium], and the molecules A–D are [Fe(Pc)(CN)$_2$]. (See Fig. 1 for the detailed molecular structure of [Fe(Pc)(CN)$_2$].) Note that θ is the angle between the magnetic field and the projection direction of the CN axis on the *ab* plane. The tilt of the projection direction from the *a* axis is approximately 59.5°.

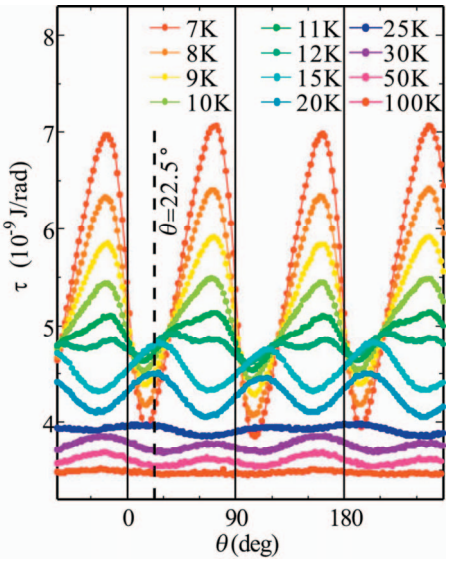

FIG. 4. (Color) The magnetic torque curve of TPP[Fe(Pc)(CN)$_2$]$_2$ measured under a magnetic field of 80 kOe rotated within the *ab* plane. Each curve has some offset for clarity. Note the torque-curve inversion at around 12 K (T_1 inversion) and above 25 K (T_2 inversion).

sign of the torque τ was defined so that a sample is dynamically in the most stable state when $\tau=0$ and $dt/d\theta>0$.

Heat capacity was measured in the temperature range between 4 and 35 K by employing the differential thermal analysis (DTA) method. Polystyrene was used as the standard. The temperature difference was measured using a Chromel-Constantan thermocouple. The magnetic field was applied parallel to the *c* axis.

III. RESULTS

A. Magnetic torque

In the paramagnetic state, the amplitude of the magnetic torque curve is proportional to the anisotropy of the magnetic susceptibility. When the magnetic field is rotated within the crystallographic *ac* plane of TPP[Fe(Pc)(CN)$_2$]$_2$, a large torque amplitude is observed, reflecting the large *g*-tensor anisotropy of [Fe(Pc)(CN)$_2$].[1] On the contrary, when the field is rotated within the *ab* plane, the torque amplitude derived from the *g*-tensor anisotropy is almost quenched due to the tetragonal symmetry of the crystal.[13] The resulting torque curve is more sensitive to the magnetic transition. In this context, we performed detailed measurements of the magnetic torque for the magnetic field rotated within the *ab* plane.

Figure 4 shows the torque curves measured under the field of 80 kOe at various temperatures above 6 K, below which spontaneous magnetization appears. Interestingly, inversions of the torque curves occur at around 12 K and just above 25 K. Here, the lower and higher temperatures of the torque inversion were defined as T_1 and T_2, respectively. These temperatures approximately coincide with those where the magnetic susceptibility (Fig. 2) exhibits anomalous behavior. We

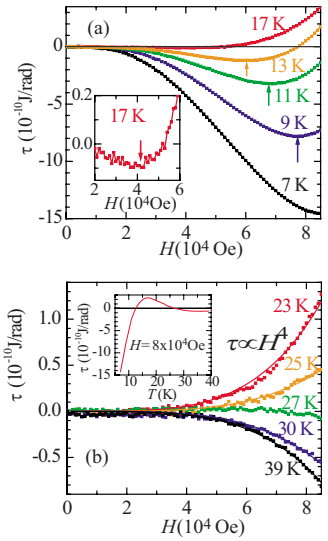

FIG. 5. (Color online) Field dependences of the magnetic torque of $TPP[Fe(Pc)(CN)_2]_2$ at $\theta=22.5°$ (a) below $T=17$ K and (b) above $T=23$ K. The data below 17 K exhibit a minimum, followed by an inversion. On the other hand, no inversion is observed above 23 K. The arrows in (a) indicate the minimum of the curve. The solid lines in (b) indicate the fit of $\propto H^4$ to the experimental data. The insets (a) and (b) show the torque minimum at 17 K and the temperature dependence, respectively.

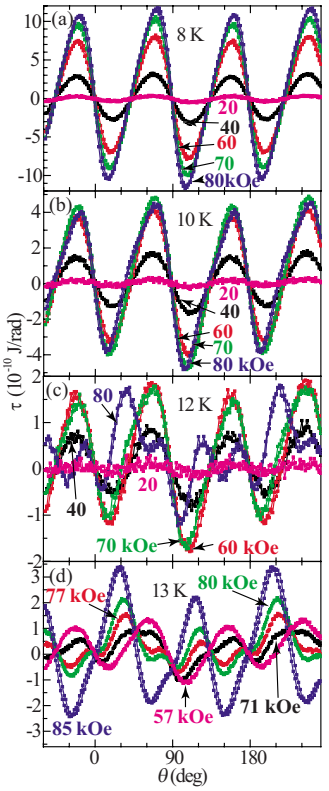

FIG. 6. (Color online) Magnetic torque curves of $TPP[Fe(Pc)(CN)_2]_2$ below $T=13$ K. Note the complicated structures of the torque curves at 12 and 13 K before the T_1 inversion.

refer to as "positive" or "negative" a torque curve on the basis of the torque amplitude at $\theta=22.5°$.

Figure 5 shows the field-strength dependence of the magnetic torque at $\theta=22.5°$ below 17 K (a) and above 23 K (b). The magnetic torque in the low-field region is negative below 17 K as shown in Fig. 5(a). As the field increases, the torque reaches a minimum and abruptly increases, finally becoming positive. As the temperature increases, the inversion takes place at lower field. Although this torque inversion is not ascertained except for the data at 13 and 17 K, the similarities between the curves suggest that it should occur as the field increases at all temperatures below $T=17$ K. Figure 5(b) shows that the T_2 torque inversion occurs around 27 K. In this temperature range, the torque is almost proportional to H^4 on both the positive and the negative sides. This indicates that the T_2 inversion is not influenced by the field strength.

Figure 6 shows the detailed measurements of torque curves at various strengths of field in the temperature range of $T \leq 13$ K, where the T_1 inversion occurs. Before describing the details of the torque curves, we should keep in mind that the twofold symmetry of the torque curves is ascribed to experimental artifacts caused by a small deviation of rotational axis from the crystallographic c axis. This symmetry is apparent in the curves at 12 and 13 K. In the following, we discuss the changes in the torque curves associated with the T_1 inversion. Because of the experimental limitation (insufficient dynamic range of a cantilever and insufficient strength of magnetic field), we could not observe all the changes given below at one temperature. (For example, we could observe the field-driven torque-curve inversion described below only at 13 K.) On the basis of the discussion for Fig. 5, however, the increase in temperature decreases the field at which the T_1 inversion occurs. By taking this into account with all the torque curves shown in Fig. 6 into consideration, we conclude that the following changes should occur when we keep constant at some temperature between 13 and 6 K and increase the magnetic field:

(1) Low-field region: In this region, the torque curve is negative, gains amplitude with the increase in the magnetic field (see the data at 8 K), and exhibits saturating behavior. (See the three torque curves for $T=10$ K at $H=60$, 70, and 80 kOe and the two curves for 12 K at $H=60$ and 70 kOe.)

(2) Intermediate-field region: In this region, the torque curve exhibits very complicated structures. (See the data for 12 K at $H=80$ kOe and the data for 13 K at $H=71$ and 77 kOe.)

(3) High-field region: Torque-curve inversion occurs. The torque curve is now positive. (See the data for $T=13$ K at $H=85$ kOe.)

Figure 7 shows the torque curves at $T=20$ and 30 K, in the temperature range around the T_2 inversion. In this temperature range, the curves have a rather simple sinusoidal shape with fourfold- and twofold-symmetry components. The latter component is ascribed to an experimental artifact, as described above. The former component at 20 K is inverted at 30 K. This figure shows that the T_2 inversion is not affected by the strength of the magnetic field. This conclusion is consistent with that given by Fig. 5(b).

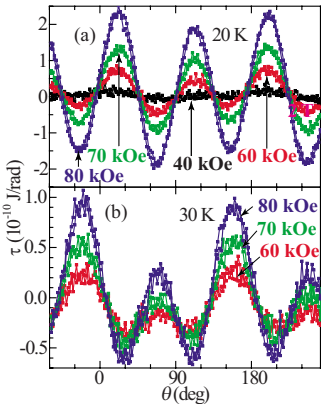

FIG. 7. (Color online) The magnetic torque curves at $T=20$ and 30 K. Note that the T_2 inversion occurs around 27 K.

B. Heat capacity

Figure 8(a) shows the temperature dependence of the heat capacity for TPP$[M(\mathrm{Pc})(\mathrm{CN})_2]_2$ (M=Fe, Co). The data of the Fe salt were measured under the fields (H=0, 40, 80, and 130 kOe) applied parallel to the c axis, while those of the Co salt were measured only at the zero field. Figure 8(b) shows ΔC, the difference in the heat capacity between the two salts. Since the Fe salt is isostructural with the Co salt,[12] the contributions of the lattice to the heat capacity are almost the same in these salts. Both salts have conduction electrons derived from the π orbital of the Pc ring. The $[\mathrm{Fe(Pc)(CN)_2}]$ unit has the $S=1/2$ local magnetic moment originating from the low-spin d^5 electrons of Fe, while the $[\mathrm{Co(Pc)(CN)_2}]$ unit has no local magnetic moment. Thus in the simplest sense, ΔC reflects the residual heat capacity due to the local magnetic moment in TPP$[\mathrm{Fe(Pc)(CN)_2}]_2$. As can be seen from the figure, ΔC reaches a maximum around 16.5 K. As the field increases, the maximum value increases. The field dependence of ΔC appears below 20 K, above which it is negligibly small. We will discuss this field dependence in Sec. IV.

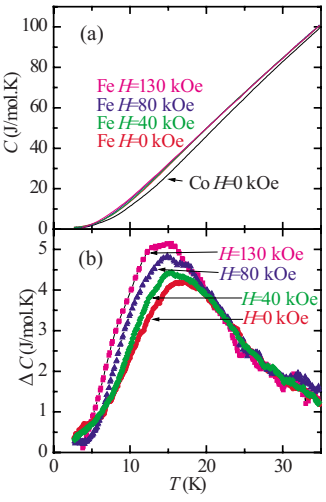

FIG. 8. (Color online) (a) Heat capacity of TPP$[M(\mathrm{Pc})(\mathrm{CN})_2]_2$ (M=Fe, Co). (b) The difference in the heat capacity between the two compounds (ΔC). The magnetic field enhances the ΔC.

The residual heat capacity ΔC is not zero even above 30 K. This suggests that the formation of a short-range order (SRO) begins at a temperature higher than 30 K. Such SRO formation at higher temperatures should be the origin of the magnetic-susceptibility peak around 25 K. In spite of the SRO formation at higher temperatures, we could detect neither a jump nor a sharp peak characteristic for a phase transition in the data of ΔC down to 4 K. In the simplest sense, this may suggest the lack of long-range order. As we show later in Sec. IV, however, the torque-curve analyses reveal the existence of a spin-flop transition of the π-electron system below 13 K. This demonstrates that the antiferromagnetic order exists at least below 13 K. One solution to this discrepancy is to consider the magnetic order grown in a one-dimensional chain. Such interpretation has been commonly accepted in quasi-one-dimensional systems. Another interpretation, recently reported, is that the anomaly in the heat capacity associated with a three-dimensional LRO is too small to be detected in a quasi-one-dimensional system.[14] In either case, one-dimensional nature is the key for the interpretation of this phenomenon.

IV. DISCUSSION

A. Anisotropic Heisenberg model in one dimension

The magnetic susceptibilities of conductive salts of $[\mathrm{Fe(Pc)(CN)_2}]$ so far reported exhibit very similar temperature dependences.[9,10] All these salts have a one-dimensional $[\mathrm{Fe(Pc)(CN)_2}]$ chain but have different crystal structures.[15] Thus, we assume that the magnetic behaviors of these salts are essentially governed by the exchange interaction within the $[\mathrm{Fe(Pc)(CN)_2}]$ chain. This assumption is consistent with the one-dimensional nature of the system discussed for the heat capacity in Sec. III B. Based on this assumption, we adopt the following anisotropic Heisenberg Hamiltonian (H) in one dimension for the analysis:

$$H = \mu_B \sum_i (g_{xx} H_x S_i^x + g_{yy} H_y S_i^y + g_{zz} H_z S_i^z) + \sum_i (J_x S_i^x S_{i+1}^x + J_y S_i^y S_{i+1}^y + J_z S_i^z S_{i+1}^z). \quad (1)$$

Here, the indices x, y, and z are rectangular coordinates, indicating the principal axes of the g tensor of the $[\mathrm{Fe(Pc)(CN)_2}]$ unit. The parameters g_{aa} and $J_\alpha (a=x,y,z)$ are the principal values of g tensor and exchange interaction, and S_i^α is the α component of the spin operator at the ith site. In the ideal $[\mathrm{Fe(Pc)(CN)_2}]$ unit, with a D_{4h} symmetry, the z axis is perpendicular to the Pc ring (parallel to the CN axis) and the x and y axes are parallel to the Pc ring. (See the definitions shown in Fig. 1.) In the crystal of TPP$[\mathrm{Fe(Pc)(CN)_2}]_2$, the $[\mathrm{Fe(Pc)(CN)_2}]$ unit loses the D_{4h} symmetry. Thus, we assumed the directions of the x, y, and z coordinates as fitting parameters.

In this model, we take into account only the contribution of unpaired d electrons with $S=1/2$ spin, neglecting the contribution of the π electrons. This approximation is justified at higher temperatures, since the π electrons form a conduction band and consequently their contribution to the magnetic

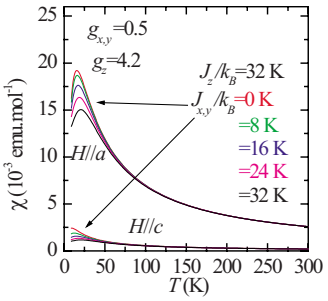

FIG. 9. (Color online) The calculation of the magnetic susceptibility as a function of temperature based on the anisotropic Heisenberg model. The definitions of parameters in the figure are given by Eq. (1) in the text.

susceptibility is negligible. We later discuss the contribution of the π electrons to magnetic properties by examining the deviation of the model calculations from the experimental results.

Since the general solution of Eq. (1) is not known, we numerically solved the equation for ring clusters with nine and ten sites and calculated the partition function Z by using

$$Z = \sum_r \exp(-\varepsilon_r/k_BT). \tag{2}$$

Here ε_r is the rth eigenvalue of the Heisenberg Hamiltonian. Free energy (F), magnetization (M), magnetic torque (τ), internal energy (U), and heat capacity (C) were calculated from the partition function based on the standard procedures given below:

$$F = -k_BT \log Z, \tag{3}$$

$$M_i = -\partial F/\partial H_i, \quad i = (x,y,z), \tag{4}$$

$$\tau = \partial F/\partial\theta, \tag{5}$$

$$U = \partial(F/T)/\partial(1/T), \tag{6}$$

$$C = \partial U/\partial T. \tag{7}$$

The results for the nine and ten sites were averaged in order to gain accuracy. This numerical calculation gave reliable results for temperatures above 10 K. We will discuss the magnetic properties based on this numerical calculation unless otherwise stated.

B. Magnetic susceptibility

Figure 9 shows the results of the calculation for the temperature dependence of the magnetic susceptibility. We used g factors of $g_{xx}=g_{yy}=0.5$ and $g_{zz}=4.2$ in this calculation. These values are roughly consistent with those determined for PNP[Fe(Pc)$(CN)_2$].[7] In order to fit the calculations to the experimental results, some adjustment of the xyz directions was necessary. In this calculation we assumed that the xy plane is 10° deviated from the Pc ring. This deviation is greater than the experimental errors. It should be noted that such deviation was also observed in the electron-spin-resonance (ESR) experiments on PNP[Fe(Pc)$(CN)_2$].[7] One of the possible origins for such deviation is the mixing of the degenerate d_{xz} and d_{yz} orbitals with π_x and π_y orbitals in the CN bond. Through this mixing, the d_{xz} and d_{yz} orbitals extend along the direction parallel to the CN axis and tend to be more influenced by the environment outside the [Fe(Pc)$(CN)_2$] unit.

As can be seen from Fig. 9, the $H\|a$ susceptibility curve in the calculation exhibits a peak at temperatures around 20 K. As we increase J_x $(=J_y)$, the peak position shifts toward a higher temperature, and the peak height is decreased. The solid lines in Fig. 2 show the results of calculation at $J_{x,y}/k_B=16$ K and $J_z/k_B=32$ K for the comparison with the experimental results. In this figure, the calculated $H\|c$ susceptibility data assume an offset of 0.5×10^{-3} emu/mol as a constant term. The consistency between the calculated and experimental susceptibilities is satisfactory above 20 K. Nevertheless, the calculation fails to explain the abrupt increase in susceptibility below 13 K. Later we will present several pieces of evidence suggesting that this increase is associated with the magnetic ordering of π electrons.

C. Magnetic torque

Figure 10 shows (a) the calculation of the torque curve and (b) the field dependence of the torque, at several temperatures. The calculation was performed in the range of $H<100$ kOe and $T>10$ K. Based on this calculation, we found the torque curves are approximated by the following equation:

$$\tau_d(H,\theta,T) = A(T)H^4 \sin(4\theta). \tag{8}$$

Here $A(T)$ is an appropriate function of temperature. When we use the parameters $J_{x,y}/k_B=16$ K and $J_z/k_B=32$ K, $A(T)$ changes sign around $T=30$ K, i.e.,

$$A(T) > 0 \quad (T \le 30 \text{ K}),$$

$$A(T) < 0 \quad (T \ge 30 \text{ K}). \tag{9}$$

The T_2 inversion phenomenon is well reproduced in this calculation. Thus, we concluded that the T_2 inversion phenomenon is caused by the SRO formation of d electrons described by Eq. (1). An intuitive explanation for this phenomenon is as follows:

(i) In the temperature range of $T\ge6$ K, no spontaneous magnetization exists. Thus, the magnetization is expanded by odd-order terms of the magnetic field.

(ii) The first-order term of the magnetic field in the expansions is extinguished due to the fourfold symmetry of the ab plane. The third-order term remains the lowest order in the expansions.

(iii) The third-order term changes its sign from positive to negative at temperatures below $T=30$ K, as can be seen from the inset of Fig. 10. This causes the torque inversion.

Next we move to the origin of the T_1 inversion phenomenon. In contrast with the T_2 inversion, the calculation based on Eq. (1) cannot explain this phenomenon. We have already described the three regions accompanying this phenomenon in Sec. III. The complicated torque curves in the

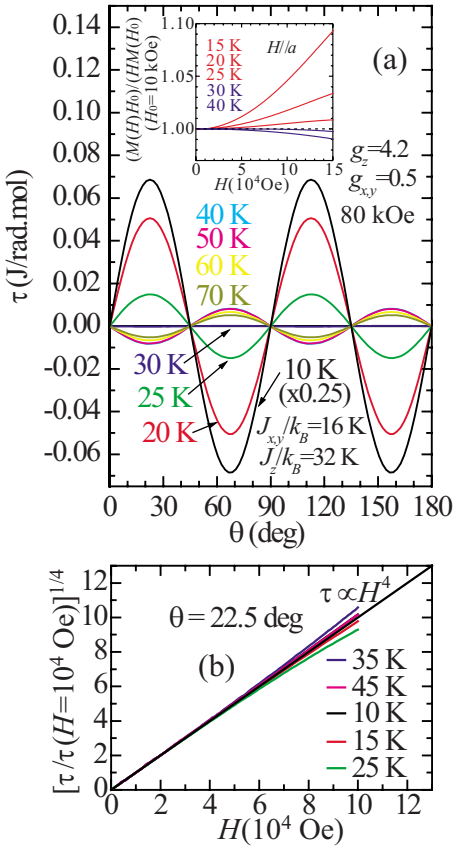

FIG. 10. (Color online) (a) Calculation of the torque curves at several temperatures. The torque-curve inversion occurs around 30 K. The inset shows the plot of $[M(H)H_0]/[M(H_0)H]$ (H_0 =10 kOe) as a function of H, indicating that the third-order term of H in the expansions of M changes sign from positive to negative upon elevating the temperature. (b) The plot of $\tau(H)/[\tau(10\ \text{kOe})]^{1/4}$ as a function of H. The calculated torque τ is almost proportional to H^4.

intermediate-field region are quite anomalous. No simple explanation for such torque curves can be offered unless we consider the contribution of π electrons in addition to the contribution of d electrons. One piece of evidence to support this consideration is the magnetic torque for the field rotated within the ac plane.[1] Because of the anisotropic g factors, these data mainly reflect the contributions of d electrons rather than those of π electrons. The data exhibit a smooth decrease in torque amplitude below 20 K and do not exhibit any anomaly associated with the abrupt increase in the susceptibility below 13 K. This implies that the abrupt increase in susceptibility is not associated with d electrons but with π electrons.

In the following discussion, we show that the T_1 inversion phenomenon can be well explained by assuming that antiferromagnetic π electrons give a negative contribution to the torque curve and that d electrons give a positive contribution. The latter assumption is plausible since the positive contribution of d electrons below T_2 is ascertained at least in Eq. (8). Since the π electrons have isotropic g factors, their contribution to the torque curve should be quite small unless some magnetic ordering exists. The negative curve indicates that the field direction of θ=0 is magnetically not stable for π electrons (see Sec. II). Thus, we assumed that π electrons form the antiferromagnetic order with an easy axis parallel to the CN axis (z axis in the g tensor). Then, we obtain the following equation for the torque curve:

$$\tau(H,\theta) = \tau_d(H,\theta) + [\tau_C(H,\theta) + \tau_D(H,\theta)]/2. \tag{10}$$

Here, $\tau_C(H,\theta)$ and $\tau_D(H,\theta)$ respectively represent the torque curve for the antiferromagnetic chains of π spins formed by molecules C and D (see Fig. 3). Using the approximation reported in Ref. 16, the former contribution is given by

$$\tau_D(H,\theta) = -\frac{\chi_\perp - \chi_\parallel}{2} H^2 \sin\left(\arctan\frac{\sin 2\theta_D}{\cos 2\theta_D - H^2\frac{\chi_\perp - \chi_\parallel}{2K_1}}\right) \times \cos\phi_D, \tag{11}$$

where $\chi_\parallel$ and $\chi_\perp$ are the magnetic susceptibilities of π spins in the antiferromagnetic state for the fields parallel and perpendicular to the easy axis, respectively, and K_1 is the anisotropic energy. The parameter θ_D is the angle between the magnetic field and the direction of easy axis of molecule D, and ϕ_D is the tilt of the torque vector of molecule D from the rotational axis (=crystallographic c axis). Using the definition of $\vec{z}_D$ as the elementary vector along the z axis of molecule D, these parameters are given by

$$\cos\theta_D = \vec{z}_D \cdot (\vec{H}/|\vec{H}|) \tag{12}$$

and

$$\cos\phi_D = \frac{\vec{H}\times\vec{z}_D}{|\vec{H}\times\vec{z}_D|} \cdot \frac{\vec{c}}{|c|}. \tag{13}$$

A similar expression can be defined for $\tau_C(H,\theta)$.

By substituting Eqs. (8) and (11) (and a similar equation for molecule C) for τ_d, τ_C, and τ_D into Eq. (10), we obtain

$$\frac{\tau(H,\theta)}{AH_c^4} = \left(\frac{H}{H_c}\right)^4 \sin 4\theta - \frac{H_0^2 H^2}{2H_c^4} \times \left\{\sum_{i=C,D}\left\{\sin\left[\arctan\frac{\sin 2\theta_i}{\cos 2\theta_i - (H/H_c)^2}\right]\right\}\cos\phi_i\right\}. \tag{14}$$

Here, H_c is a spin-flop field defined as

$$H_c = \left(\frac{2K_1}{\chi_\perp - \chi_{//}}\right)^{1/2}, \tag{15}$$

and H_0 is defined as

$$H_0 = \left(\frac{\chi_\perp - \chi_\parallel}{4A}\right)^{1/2}. \tag{16}$$

Figure 11(a) shows a simulation based on Eq. (14) at H_c/H_0=0.3. In a low field ($H<H_c$), the torque curve exhibits negative behavior, reflecting antiferromagnetic ordering of π electrons, and the torque curve abruptly grows up. At the field of $H=H_c$, the torque curve is almost saturating and then gradually becomes depressed. The lack of a jump of the

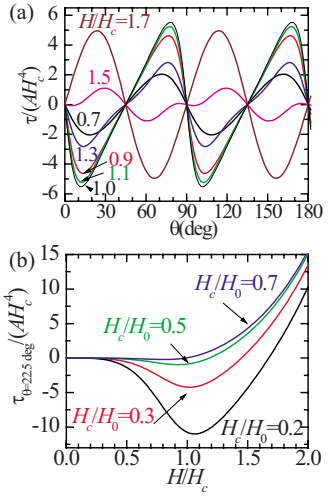

FIG. 11. (Color online) (a) The simulation of the torque curve based on Eq. (14) at $H_c/H_0=0.3$. (b) Field dependence of the torque amplitude calculated using Eq. (14).

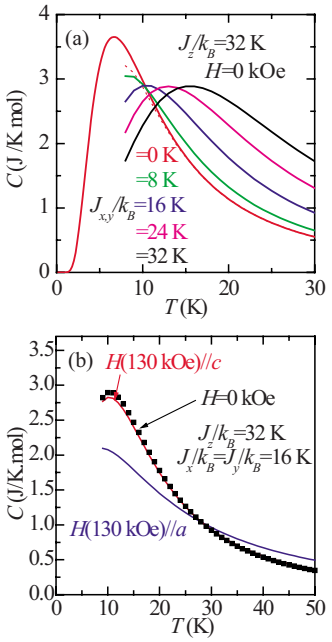

FIG. 12. (Color online) (a) Calculations of the heat capacity based on the anisotropic Heisenberg model in one dimension. The calculations at $J_{x,y}=0$ are the results of an exact solution based on the Ising model. The red dotted line indicates the results of the numerical calculation for the same Ising model. (b) The calculation of the heat capacity under the applied magnetic field for the anisotropic Heisenberg model ($J_z/k_B=32$ K; $J_{x,y}/k_B=16$ K). The squares indicate the calculations at the zero field. The heat capacity is seriously depressed for $H\|a$, but it is almost unchanged for $H\|c$.

torque curve at $H=H_c$ comes from the deviation of the easy axis from the *ab* plane, on which the magnetic field is rotated. As we continue to increase the field, the contribution of π electrons competes with that of *d* electrons and the complicated torque curve appears [$H\sim1.5H_c$ in Fig. 11(a)]. Finally, a sinusoidal torque curve due to the *d*-electron system becomes dominant [$H=1.7H_c$ in Fig. 11(a)]. All these behaviors are consistent with the observation described in Sec. III A.

Figure 11(b) shows the field dependence of the magnetic torque. The calculation demonstrates that the spin-flop field of the π-electron system H_c is approximately given by the field where the torque at $\theta=22.5°$ exhibits a minimum. Experimentally, this field is shown by the arrows in Fig. 5(a) (for example, ~80 kOe at $T=9$ K). Thus, the evaluated fields are more than ten times higher than the corresponding values of typical organic magnets. This suggests the large d-π coupling in this system. We should note a small dip appearing on the curve at $T=17$ K in the inset of Fig. 5(a). This suggests that antiferromagnetic fluctuation of π electrons survive even at this temperature.

This simulation explains the T_1 torque inversion phenomenon completely. Thus, we conclude that internal field due to the antiferromagnetic order is formed in the π-electron system below 13 K. A problem with this model is the abrupt increase in magnetic susceptibility below 13 K. Since the susceptibility in the antiferromagnetic state should decrease as the temperature is lowered, one may consider that this model is inconsistent with the experimental results. Although a definite answer to this argument is not known at the present stage, we are considering that the π-electron system is not in a genuine antiferromagnetic state. If we assume a parasitic ferromagnetism, it should exhibit a torque curve similar to the antiferromagnetic state, while the magnetic susceptibility should increase as the temperature is lowered. In any case, more detailed studies are necessary in order to solve this problem.

D. Heat capacity

Figure 12(a) shows the results of calculation for the heat capacity at the zero magnetic field. In the case of $J_x=J_y=0$ (Ising model), the peak value of the heat capacity is ~3.65 J/K mol. As we increase J_x ($=J_y$), the value decreases and finally converges into ~2.89 J/K mol (Heisenberg model). Although the observed peak value, ΔC ~4.2 J/K mol, is close to that of Ising model rather than that of anisotropic Heisenberg model, we cannot conclude at present which model is appropriate. Their differences are within experimental error. Moreover, we should recognize that the comparison is possible only when the roles of the π conduction electrons are exactly the same in both TPP[Fe(Pc)$(CN)_2]_2$ and TPP[Co(Pc)$(CN)_2]_2$.

Figure 12(b) shows the calculations of the heat capacity under the magnetic field. The calculations are shown only for the anisotropic Heisenberg models. As can be seen from the figures, the heat capacity is almost unchanged for the field of 130 kOe along the *c* axis. This is due to the smallness of the g_{xx} and g_{yy} values. On the contrary, the heat capacity is seriously depressed when the field is applied along the *a* axis. This conclusion is the same for both the Ising and the anisotropic Heisenberg models.

As shown in Fig. 8(b), enhancement of the heat capacity is observed for the magnetic field applied parallel to the *c* axis. This is apparently inconsistent with the calculations. This enhancement may be explained by taking into account

the magnetic ordering which has been pointed out in Sec. IV C for π electrons. From the field dependence, we speculate that the fluctuation of this ordering begins just below 20 K.

Here, one may ask why this fluctuation is sensitively detected in the heat capacity measurements. In the case of magnetic properties, the contribution of *d* electrons overwhelms that of π electrons because *d* electrons have anomalously large *g* factors. On the contrary, the *g* factor does not seriously affect the heat capacity unless the magnetic field is applied. Thus, the contributions of *d* electrons and π electrons are essentially equivalent in the heat capacity. This is the reason why we could sensitively detect the magnetic fluctuation of π electrons in the heat capacity measurements.

E. Possible mechanism of GNMR

At the end of this paper, we briefly discuss the possible mechanism of GNMR in $TPP[Fe(Pc)(CN)_2]_2$ salt. This salt is a one-dimensional conductor with a quarter-filled band. Although the antiferromagnetic order of the *d*-electron system induces additional periodic potential on the π-electron system through the d-π interaction, the periodicity is $4k_F(\pi/c)$, which does not open the gap at the Fermi level. Thus we cannot simply ascribe the semiconducting behavior to the antiferromagnetic SRO formation of *d* electrons.

At the present stage, we are considering that the formation of the magnetic domain wall in the one-dimensional chain is the most plausible origin of the semiconducting behavior. In this context, we should recall the parasitic ferromagnetism of the π-electron system discussed in Sec. IV C. If the fluctuation of such parasitic ferromagnetism exists at higher temperatures, the applied external magnetic field should enlarge the domain size and decrease the resistivity.

Another possible mechanism is to consider the double-exchange interaction that is the origin of GNMR in manganese oxides.[4] At the present stage, however, we think this mechanism is not appropriate for $TPP[Fe(Pc)(CN)_2]_2$. The reason is as follows: In order to apply this mechanism to $TPP[Fe(Pc)(CN)_2]_2$, large canting of the *d* spin is necessary. Considering the anisotropic nature of *d* spins, however, such canting is not plausible. In any case, more studies are necessary in order to clarify the mechanism of GNMR in this system.

V. CONCLUSIONS

In summary, we found that the magnetic behavior of *d* electrons in $TPP[Fe(Pc)(CN)_2]_2$ above 10 K is well explained by the anisotropic Heisenberg model in one dimension. We could detect neither a jump nor a sharp peak characteristic for a phase transition in the heat capacitance measurements down to 4 K, suggesting the one-dimensional nature of the system. Based on the torque-curve analysis, we found that π electrons fall into an antiferromagnetic state below 13 K with an easy axis parallel to the CN axis of $[Fe(Pc)(CN)_2]$. The estimated spin-flop field of the π-electron system is approximately 80 kOe at 9 K. Such large spin-flop field is indicative of the large d-π interaction in this system.

ACKNOWLEDGMENTS

The authors acknowledge valuable discussion with M. Takigawa at ISSP. This work was supported by Grants-in-Aid for Scientific Research on Priority Areas of "Molecular Conductors" (No. 15073207) and of "Invention of Anomalous Quantum Materials—New Physics through Innovative Materials" (No. 19014015) from the Ministry of Education, Culture, Sports, Science and Technology of Japan and a Grant-in-Aid for Scientific Research (B: No. 18350070) from the Japan Society for the Promotion of Science.

[1] N. Hanasaki, H. Tajima, M. Matsuda, T. Naito, and T. Inabe, Phys. Rev. B **62**, 5839 (2000).
[2] N. Hanasaki, M. Matsuda, H. Tajima, E. Ohmichi, T. Osada, T. Naito, and T. Inabe, J. Phys. Soc. Jpn. **75**, 033703 (2006).
[3] C. Hotta, M. Ogata, and H. Fukuyama, Phys. Rev. Lett. **95**, 216402 (2005).
[4] Y. Tokura, A. Urushibara, Y. Moritomo, R. Arima, A. Asamitsu, G. Kido, and N. Furukawa, J. Phys. Soc. Jpn. **63**, 3931 (1994).
[5] F. Goze, V. N. Laukhin, L. Brossard, A. Audouard, J. P. Ulmet, S. Askenazy, T. Naito, H. Kobayashi, A. Kobayashi, M. Tokumoto, and P. Cassoux, Europhys. Lett. **28**, 427 (1994).
[6] M. Matsuda, N. Hanasaki, H. Tajima, T. Naito, and T. Inabe, J. Phys. Chem. Solids **65**, 749 (2004).
[7] N. Hanasaki, M. Matsuda, H. Tajima, T. Naito, and T. Inabe, J. Phys. Soc. Jpn. **72**, 3226 (2003).
[8] In this paper, we define $TPP_{0.5}[FePc(CN)_2]$ as the unit of "mol."
[9] M. Matsuda, T. Asari, T. Naito, T. Inabe, N. Hanasaki, and H. Tajima, Bull. Chem. Soc. Jpn. **76**, 1935 (2003).
[10] M. Matsuda, T. Naito, T. Inabe, N. Hanasaki, and H. Tajima, J. Mater. Chem. **11**, 2493 (2001).
[11] E. Ohmichi and T. Osada, Rev. Sci. Instrum. **73**, 3022 (2002).
[12] M. Matsuda, T. Naito, T. Inabe, N. Hanasaki, H. Tajima, T. Otsuka, K. Awaga, B. Narymbetov, and H. Kobayashi, J. Mater. Chem. **10**, 631 (2000).
[13] N. Hanasaki, M. Matsuda, H. Tajima, T. Naito, and T. Inabe, Synth. Met. **137**, 1227 (2003).
[14] T. Lancaster, S. J. Blundell, M. L. Brooks, P. J. Baker, F. L. Pratt, J. L. Manson, C. P. Landee, and C. Baines, Phys. Rev. B **73**, 020410 (2006).
[15] T. Inabe and H. Tajima, Chem. Rev. (Washington, D.C.) **104**, 5503 (2004).
[16] H. Ozaki, H. Ohya-nishiguchi, and J. Yamauchi, Phys. Lett. **54A**, 227 (1975).